Polymer Testing 56 (2016) 65–73

Contents lists available at ScienceDirect

Polymer Testing

journal homepage: www.elsevier.com/locate/polytest

Material Properties

Nano lithium aluminate filler incorporating gel lithium triflate polymer composite: Preparation, characterization and application as an electrolyte in lithium ion batteries

Emad M. Masoud

Chemistry Department, Faculty of Science, Benha University, 13518 Benha, Egypt

A R T I C L E I N F O

Article history:
Received 19 July 2016
Received in revised form
13 September 2016
Accepted 22 September 2016
Available online 23 September 2016

Keywords:
Polymer nano composites electrolytes
Lithium ion batteries
Electrical properties
Complex impedance

A B S T R A C T

Gel polymer composites electrolytes containing nano $LiAlO_2$ as filler were prepared using a solution cast technique and characterized using different techniques such as X-ray diffraction (XRD), thermal analysis (TG, DSC), Fourier transform infra – red spectroscopy (FT-IR) and scanning electron microscope (SEM). X-ray diffraction analysis showed the effect of lithium tri fluoro methane sulphonate ($LiCF_3SO_3$), poly vinyl acetate (PVAc) and nano lithium aluminate ($LiAlO_2$) on the crystalline structure of the poly vinylidene fluoride –co– hexa fluoro propylene (PVDF-co-HFP) matrix containing ethylene carbonate (EC) and diethyl carbonate (DEC) as plasticizers. FT-IR analysis confirmed both the good dissolution of the $LiCF_3SO_3$ salt and the good interaction of the nano $LiAlO_2$ filler with the polymer matrix. TG analysis showed the good thermal stability of the $LiAlO_2$ samples compared to the free one. Also, addition of nano $LiAlO_2$ filler enhanced the conductivity value of the polymer composites electrolytes. The sample containing 2 wt% of $LiAlO_2$ showed the highest conductivity value, $4.98 \times 10^{-3}\ \Omega^{-1}\ cm^{-1}$ at room temperature, with good thermal stability behavior ($T_d = 362$ °C). This good conductive and thermally stable polymer nano composite electrolyte was evaluated as a promising membrane for lithium ion batteries application.

1. Introduction

Increasing interest for high energy density solid state batteries has been pushing many researchers to explore new concepts and related materials. Most promising options seem to be given by lithium-ion technology employing polymer electrolytes as the separator of rechargeable batteries [1]. Poly(vinylidene fluoride-co-hexafluoropropylene) P[(VdF-HFP)] has received attention due to its good thermal and electrochemical stability [2]. This copolymer has amorphous phase favoring ionic conduction, and at the same time crystalline PVdF phase acts as a mechanical support [3]. This satisfies the two contradictory properties of high ionic conduction and good mechanical strength. Recently, P(VdF-HFP) has shown potential as a polymer electrolyte material of rechargeable lithium batteries due to its high solubility, low crystallinity and glass transition temperature [4]. Many researchers present good results for P(VdF-HFP)-based polymer electrolytes with different types of dopant salts, such as lithium fluoro alkyl phosphate [5], lithium perchlorate [6] and lithium bis (trifluoro methane sulfonyl) imide [7].

According to Ratner and Shriver [8], the conduction of ions in the polymer electrolyte takes place mainly in the amorphous region. PVAc has an amorphous structure and its addition with a small amount will reduce the crystalline nature of the host polymer as it helps to improve the conductivity. The possibility of using PVAc/PVdF-co-HFP based polymer blend electrolytes for rechargeable lithium batteries has been investigated by Choi et al. [9]. To increase the conductivity value at room temperature, considerable research work has been carried out on various polymers using different approaches, such as blending of two polymers [10,11], addition of plasticizers (such as Ethylene carbonate, EC and Diethyl carbonate, DEC) to get gel polymer electrolytes [12] and addition of fillers to get composite electrolytes [13].

Addition of a small-particle size ceramic powder such as ZrO_2, TiO_2, Al_2O_3, etc., in the gel polymer electrolytes to get composite gel polymer electrolytes was one of the most important methods to enhance the conduction process [14–17].

As a part of our previous work [18], effect of $LiAlO_2$, as a nano filler, was studied on structure and electrical properties of PEO-

---

E-mail addresses: emad.youssef@fsc.bu.edu.eg, emad_masoud1981@yahoo.com.

http://dx.doi.org/10.1016/j.polymertesting.2016.09.024
0142-9418/

$LiClO_4$. The filler showed a good effect on the lithium –ions motion and a good ionic conductivity value at room temperature. In this paper, for the first time, we also try to use the same filler to enhance the electrical properties of PVDF-co-HFP and improve its performance in presence of PVA_C, EC-DEC, and lithium tri fluoro methane sulphonate, $LiCF_3SO_3$ as a salt.

2. Experimental

Materials: pure reagent materials of $LiNO_3$ (purity 99%, Merck), $Al(NO_3)_3$ (purity 99%, Merck), Citric acid ($C_6H_8O_7$, purity 98%, Fluke), PVAc (Sigma – Aldrich, 99.99%), P(VdF-co-HFP) (Sigma – Aldrich, 99.99%), Ethylene carbonate (Sigma – Aldrich, 99.99%), Diethyl carbonate (Sigma – Aldrich, 99.99%), $LiCF_3SO_3$ (Sigma – Aldrich, 99.99%).

2.1. Preparation of nano $LiAlO_2$ filler

Lithium aluminate nano particles filler was prepared by citrate – based sol - gel method [19]. 0.5 mol lithium nitrate and 0.5 mol aluminium nitrate were firstly dissolved in 300 ml distilled water, then 1 mol citric acid was added to the above solution. The molar amount of citric acid was equal to total molar amount of metal nitrates in the solution. Ammonium hydroxide was slowly added to adjust the P^H value of the solution in the range of 8–9 and also to stabilize the nitrate – citrate solution. During this procedure, the solution was kept at room temperature and continuously stirred. The obtained transparent sol was kept overnight at 80 °C to get a gel, which was then dried at 110 °C for 10 h. Finally, the precursor powder was calcinated at 950 °C for 6 h.

2.2. Preparation of polymer nano composites electrolytes

Firstly, the polymer composites electrolytes were prepared using a simple solution casting technique. The two polymers (PVAc, PVDF-co-HFP) were first dissolved in an equal volume mixture of tetra hydro furan (THF) and di-methyl formamide (DMF) under heating (40 °C). The given amounts of plasticizers (EC: DEC, 1:1 in volume) were then added into the above polymers mixture. After that, $LiCF_3SO_3$ salt was added according to the following concentrations:

$$[6.25(\mathrm{PVAc}) + 26.75(\mathrm{PVDF-co-HFP}) + 67(\mathrm{EC-DEC})] + x(\mathrm{LiCF_3SO_3}),\ x = 0, 2, 4, 6, 8\,\mathrm{wt.\%}$$

The obtained homogenous viscous slurry was poured into a Petri dish. The solvent was allowed to evaporate slowly from the composite at room temperature for three days and then all samples were dried at 50° C for 4 h s.

Secondly, the polymer nano composites electrolytes were prepared by nano filler $LiAlO_2$ addition to the optimized polymer composite electrolyte using the same method and according to the following concentrations:

$$[(\mathrm{PVAc}) + (\mathrm{PVDF-co-HFP}) + (\mathrm{EC-DEC}) + (\mathrm{LiCF_3SO_3})] + x(\mathrm{LiAlO_2}),\ x = 0, 2, 4, 6, 8\,\mathrm{wt.\%}$$

The slurry was continuously stirred for 24 h to avoid filler aggregation and get a good mixing. The obtained homogenous viscous slurry was poured into the Petri dish. The solvent evaporation was performed as mentioned above to get the electrolytes membranes (340–360 μm).

At last, the sample containing PVAc, PVDF-co-HFP, EC and DEC was denoted as BPC (blank polymer composite); the sample containing PVAc, PVDF-co-HFP, EC, DEC and optimized salt concentration was denoted as BOPCE (blank optimized polymer composite electrolyte); and the sample containing PVAc, PVDF-co-HFP, EC, DEC, optimized salt concentration and optimized filler was denoted as OPNCE (optimized polymer nano composite electrolyte).

2.3. Characterizations

X-ray diffraction analysis was performed on a Diano (made by Diano Corporation, U.S.A.) with Cu-filtered CuKα radiation (λ = 1.5418 Å) energized at 45 kV, and 10 mA. The samples were measured at room temperature in the range from 2θ = 0° to 80°. Differential scanning calorimetry (DSC) and thermal gravimetric analysis (TG) were performed in air atmosphere with a constant heating rate of 10 °C/min. in a temperature range of 298–523 K (for polymer composites electrolytes) and 298–873 K (for polymer nano composites electrolytes) using Shimadzu DSC-60H. The Fourier transform infra red spectra of the samples were recorded in the range of 625–4000 cm^{-1} using a Brucker - FT-IR. Scanning electron microscopy was carried out with JOEL scanning electron microscope (JSM-35CF). The thickness of each sample was measured using a micrometer screw gauge. Ionic conductivity(from 298 to 388 K) and complex impedance (from 100 Hz -1 MHZ) measurements of the polymer nano composites electrolytes were performed with the help of stainless steel blocking electrodes using a programmable automatic LCR bridge (Model RM 6306 Phillips Bridge). Battery performance test of the optimized polymer nano composite electrolyte (OPNCE) was conducted by fabricating a swagelok cell with $LiFePO_4$ cathode and lithium metal anode. The cathode was made by mixing $LiFePO_4$ (active material, Aldrich), (80 wt.%), with carbon black (10 wt.%) and PVDF (10 wt.%) in presence of n-methylpyrrolidinone to make the mixture homogeneous and then the mixture was left on a stirrer for 2 h to get a homogeneous material (Slurry). Then, the mixed slurry was deposited on a thin aluminium foil by a doctor blade process and dried at 80 °C for 2 h afterward. The covered aluminium foil was finally punched into round pieces with a diameter of 12 mm and transferred into a glove box (moisture content is less than 4 ppm) for battery assembly. The anode electrode used in the half cell was lithium foil. The cell was galvanostatically charged and discharged using EG&G Electrochemical analyzer (Model – 6310) in the scan rate of 1 mV^{-1} to perform charge – discharge processes for the assembled battery. The charge –discharge processes were performed at a voltage between 2.5 and 4 V and a rate of 0.2C.

3. Results and discussion

3.1. Effect of $LiCF_3SO_3$ addition on BPC

3.1.1. X-ray analysis

X-ray diffraction patterns of PVAc, PVDF-co-HFP, $LiCF_3SO_3$, BPC and BPC containing different $LiCF_3SO_3$ concentrations (2, 4, 6, and 8 wt%) are displayed in Fig. 1. As we can see, the amorphous nature of PVAc was observed. The XRD pattern of the PVdF-co-HFP polymer confirmed its semi crystalline nature [20]. The absence of the characteristic crystalline peaks of PVdF-co-HFP in the BPC sample confirms the good effect of PVAc on the semi crystalline structure of PVdF-co-HFP. More notably, the sharp crystalline peaks of $LiCF_3SO_3$ disappeared in the samples of $LiCF_3SO_3$ containing BPC to show the good dissolution behavior of the $LiCF_3SO_3$ in the PVdF-co-HFP matrix structure. By a close inspection, one can also observe that the sample containing 8 wt% of $LiCF_3SO_3$ has less crystalline structure than the other ones, as no crystalline peaks can be observed.

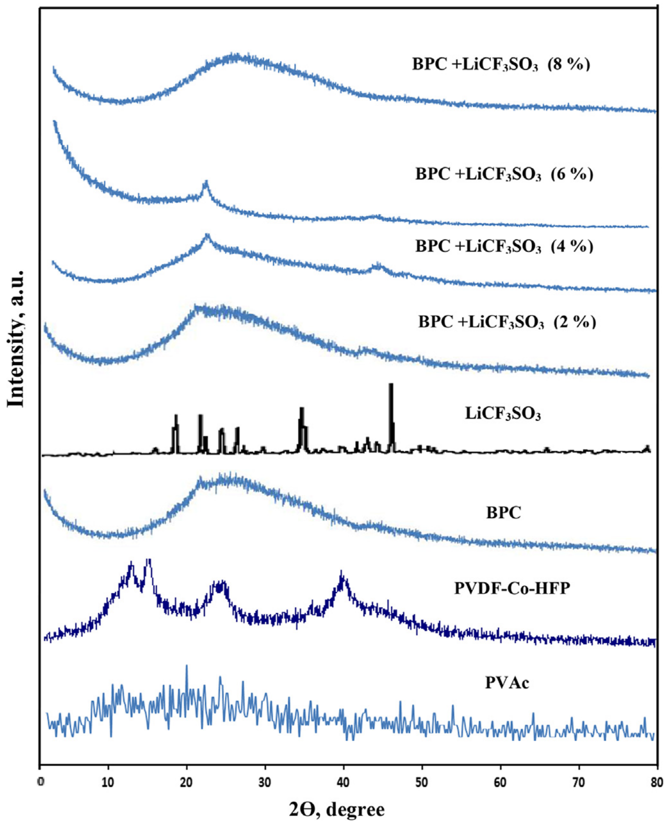

Fig. 1. X-ray diffraction patterns of PVAC, PVDF-Co-HFP, BPC, $LiCF_3SO_3$ and BPC containing different concentrations of $LiCF_3SO_3$ (2, 4, 6, 8 wt %).

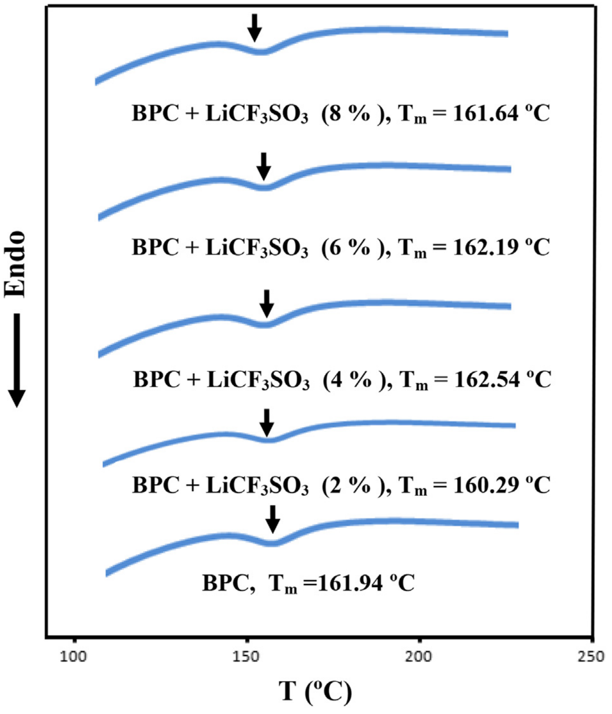

Fig. 2. Differential scanning calorimetry (DSC) of BPC and BPC containing different concentrations of $LiCF_3SO_3$ (2, 4, 6, 8 wt %).

Table 1
Values of melting temperature (T_m), heat enthalpy of melting (ΔH_m) and crystallinity percent (X_c) of BPC and BPC containing different concentrations of $LiCF_3SO_3$ (2, 4, 6, 8 wt %).

Sample	T_m,°C	ΔHm, J/g	X_c, %
BPC	161.94	4.44	4.24
BPC - $LiCF_3SO_3$ (2 wt %)	160.29	7.69	7.34
BPC - $LiCF_3SO_3$ (4 wt %)	162.54	6.88	6.57
BPC - $LiCF_3SO_3$ (6 wt %)	162.19	8.93	8.53
BPC - $LiCF_3SO_3$ (8 wt %)	161.64	3.16	3.02

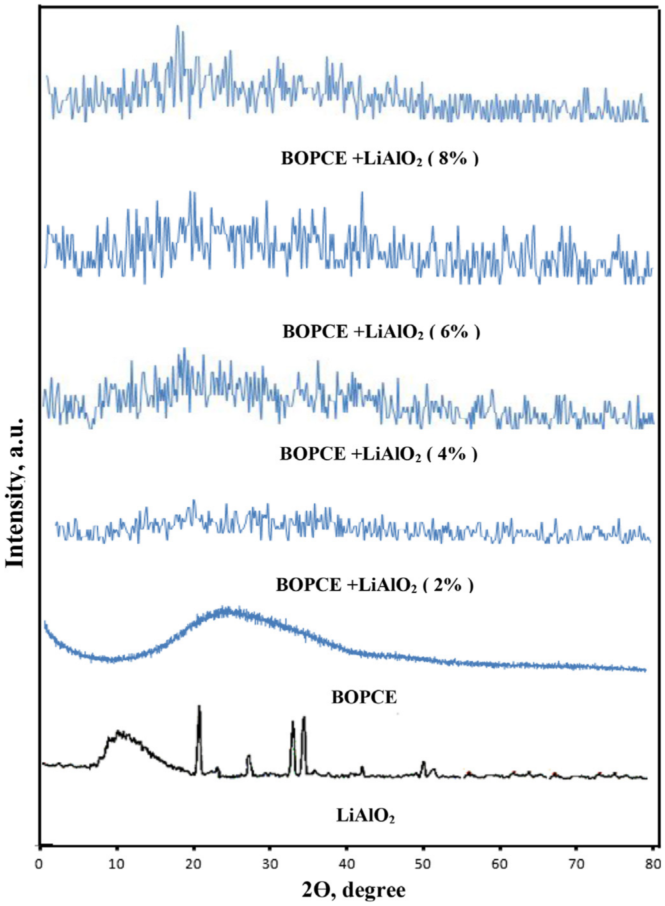

Fig. 3. X-ray diffraction patterns of $LiAlO_2$, BOPCE and BOPCE containing different concentrations of $LiAlO_2$ (2, 4, 6, 8 wt %).

3.1.2. *Differential scanning calorimetry (DSC) analysis*

DSC thermograms of BPC and BPC containing different concentrations of $LiCF_3SO_3$ (2, 4, 6, 8 wt%) are shown in Fig. 2. The crystallinity relative percentage (X_C) has been calculated using the equation [21]:

$$X_c = \Delta H_c / \Delta H_p \qquad (1)$$

Where ΔH_p equals to 104.7 J/g which is the heat enthalpy of 100% crystalline PVDF [22], and ΔH_c is the heat enthalpy of BPC and BPC containing different concentrations of $LiCF_3SO_3$. The calculated relative crystallinity (X_C) and the data obtained from DSC thermograms are shown in Table 1. The sample containing 2 wt% of $LiCF_3SO_3$ has a lower melting temperature value (T_m = 160.29 °C) compared to the others. On the other hand, the crystallinity relative percentage (X_C) also showed an irregular

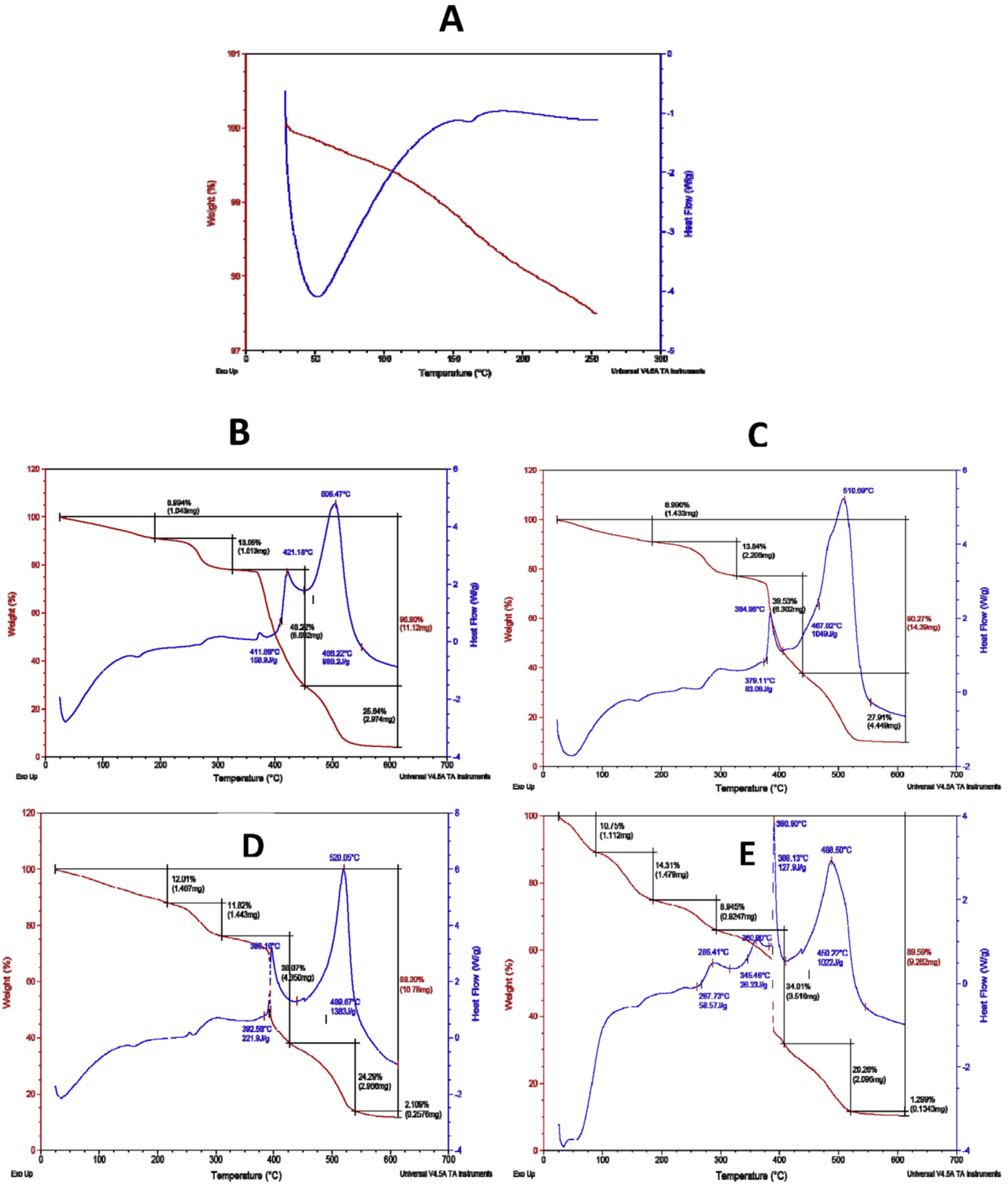

Fig. 4. Thermal analysis (TG-DSC) of BOPCE (A) and BOPCE containing different concentrations of $LiAlO_2$: (B) 2 (C) 4 (D) 6 and (E) 8 wt %.

trend, the sample containing 8 wt% of $LiCF_3SO_3$ has the lowest crystallinity value ($X_C = 3.02\%$). Here, it is a worthwhile to mention that this low crystalline value confirms what was observed before by X-ray diffraction, the same sample showed no crystalline peaks.

3.2. *Effect of $LiAlO_2$ addition on BOPCE*

3.2.1. *X-ray analysis*

X-ray diffraction patterns of $LiAlO_2$, BOPCE and BOPCE containing different nano $LiAlO_2$ concentrations (2, 4, 6, and 8 wt%) are

Table 2
Values of melting temperature (T_m), heat enthalpy of melting (ΔH_m), crystallinity percent (X_c), decomposition temperature (T_d), ionic AC- conductivity (σ_{AC}) and activation energy (E_a) of BOPCE and BOPCE containing different concentrations of $LiAlO_2$ (2, 4, 6, 8 wt%).

Sample	T_m, °C	ΔH_m, J/g	X_c,%	T_d, °C	σ_{AC} ($ohm^{-1}\ cm^{-1}$) at 298 K	E_a, eV
BOPCE	161.64	3.16	3.02	185	1.26×10^{-4}	0.14
BOPCE - $LiAlO_2$ (2 wt%)	161.24	8.71	8.32	362	4.98×10^{-3}	0.07
BOPCE - $LiAlO_2$ (4 wt%)	160.90	9.03	8.62	380	2.98×10^{-3}	0.11
BOPCE - $LiAlO_2$ (6 wt%)	160.65	8.83	8.43	387	3.01×10^{-3}	0.10
BOPCE - $LiAlO_2$ (8 wt%)	159.16	10.59	10.11	262	1.50×10^{-3}	0.12

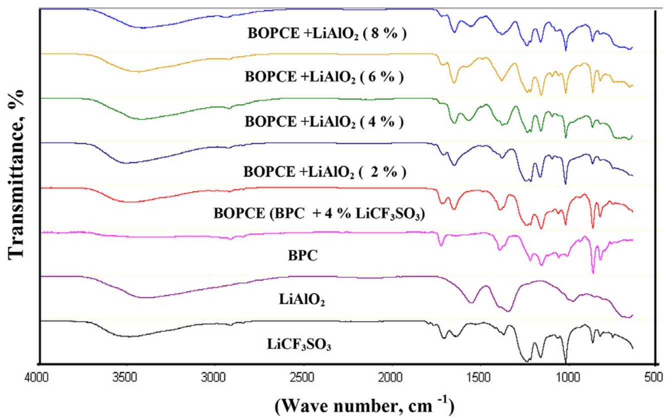

Fig. 5. FT-IR spectra of $LiCF_3SO_3$, $LiAlO_2$, BPC, BOPCE and BOPCE containing different concentrations of $LiAlO_2$ (2, 4, 6, 8 wt %).

displayed in Fig. 3. The pattern of $LiAlO_2$ is a typical XRD pattern for $LiAlO_2$ with a tetragonal structure as indexed in the standard data (JCPDS card No. 74–2232, a = 2.800 Å and c = 14.21 Å) [23]. XRD line broadening was used to estimate the crystallite size of the powder according to Scherrer formula [24]:

$$D = 0.9\ \lambda/\beta\ \cos\theta \tag{2}$$

Where λ is the wavelength of x-ray, θ is the Bragg angle and β is the full width half maximum in radians. The results showed an average crystallite size of about 41 nm.

Also, from the figure, we can observe the effect of nano $LiAlO_2$ filler addition on BOPCE sample as its broad hump was completely disappeared, confirming the ability of nano $LiAlO_2$ to create a more amorphous structure, through Lewis acid - base interactions between the filler surface and the polar fluoride atom (F) of PVDF-co-HFP. Moreover, one can observe that the sample containing 2 wt% of $LiAlO_2$ has low intensive peaks compared to the other different $LiAlO_2$ concentrations samples, demonstrating the low crystalline structure.

3.2.2. Differential scanning calorimetry (DSC) and thermal gravimetric (TG) analyses

DSC and TG thermograms of BOPCE and BOPCE containing different nano $LiAlO_2$ concentrations (2, 4, 6, 8 wt%) are shown in Fig. 4. The (X_c) has also been calculated using equation (1). The data obtained from DSC thermograms are shown in Table 2. The table showed that melting temperature (T_m) of BOPCE continuously decreases by addition of $LiAlO_2$ to show that the sample containing 8 wt% of $LiAlO_2$ has the low value ($T_m = 159.16$ °C) compared to the others. The crystallinity relative percentage (X_C) values also showed an irregular trend like what observed by $LiCF_3SO_3$ samples, where the sample containing 2 wt% of $LiAlO_2$ has the low value ($X_C = 8.32\%$), as also approved by x-ray diffraction analysis.

To further show the effect of nano $LiAlO_2$ filler addition on the thermal decomposition of the BOPCE composite, thermal gravimetric (TG) analysis was also investigated, Fig. 4.

For the $LiAlO_2$ free sample (Fig. 4A), the TG analysis was only performed till 250 °C to exactly show the start of the sample decomposition, and to determine its accurate temperature value. After that, all the other samples were analyzed till 600 °C to explore the thermal stability of all samples in presence of nano $LiAlO_2$ filler.

It is observed from Fig. 4 A that there is a preliminary weight loss in the temperature range of room temperature −150 °C. This can be attributed to the removal of moisture and/or the absorbance of water by the sample during the loading and the weight loss is in agreement with the endothermic peak observed in the DSC curve. The sample starts to melt at 161.64 °C (another endothermic peak was also observed, DSC). The determined total weight loss till melting temperature was about 1.5%. After that, the sample starts to decompose at 185 °C.

For all the other samples (except for BOPCE sample containing 8 wt.% of $LiAlO_2$), the same behavior was observed with a temperature increase shift of all preliminary changes (removal water, melting) and decomposition, confirming the good thermal stability of all $LiAlO_2$ BOPCE samples. All values of decomposition temperatures (T_d) of all samples were shown in Table 2. It is obvious from the table that the BOPCE sample containing 6 wt% of $LiAlO_2$ has the highest value (387 °C) and that containing 8 wt% of $LiAlO_2$ has the lowest one (262 °C). The decomposition weight loss was mainly due to the degradation of the side chains of the polymers. This was confirmed by the exothermic peaks observed through the DSC curves. The different remaining weight percentage of all analyzed samples could be due to the presence of $LiAlO_2$ or due to the presence of −CF based back bones of the PVdF-co-HFP polymer [25].

3.3. FT-IR analysis

Fig. 5 shows the FT-IR transmittance spectra of $LiCF_3SO_3$, $LiAlO_2$, BPC, BOPCE and BOPCE containing different nano $LiAlO_2$ concentrations (2, 4, 6, 8 wt %). The BPC sample showed different bands characteristic to PVAc or PVDF-co-HFP [25], Table 3. All changes of frequency characteristics of BOPCE and BOPCE containing different $LiAlO_2$ concentrations are also shown in Table 3. The table showed that some bands of BPC were shifted to higher or lower wave numbers in presence of the salt (BOPCE) and the different concentrations of $LiAlO_2$ filler, confirming the interactions between the BPC, salt and filler. Another important notice is that the characteristic peak of $LiAlO_2$ filler appears at 1562 cm^{-1} was also shifted in some $LiAlO_2$ composites (4, 6, 8 wt%) and only disappeared for the 2 wt % one, to confirm the interactions.

3.4. Scanning electron microscope (SEM)

To explore the nano $LiAlO_2$ filler particles distribution within the PVDF-co-HFP matrix, scanning electron microscope photographs of BOPCE and BOPCE containing 2 wt % of $LiAlO_2$ (OPNCE) were obtained, Fig. 6 (A,B). One can notice the porous structure of the PVDF-

Table 3
FT-IR spectral bands assignment of BPC, BOPCE and BOPCE containing different $LiAlO_2$ concentrations.

Wave number (cm^{-1})	Band assignment					
	BPC	BOPCE	2 wt% $LiAlO_2$	4 wt% $LiAlO_2$	6 wt% $LiAlO_2$	8 wt% $LiAlO_2$
799	C–H wagging of PVAc	803	805	807	809	804
947	–CH bending of PVAc	954	946	946	946	946
1033	C–O stretching of PVAc	1039	1039	1046	1048	1049
1243	C–O–C stretching of PVAc	1249	1248	1248	1248	1248
1373	CH_3 symmetric bending of PVAc	1373	1368	1368	1376	1377
1734	C=O stretching of PVAc	1745	1745	1758	1758	1761
2933	CH_3 asymmetric stretching of PVAc	2939	2941	2941	2941	2943
763	Crystalline phase VdF unit of PVDF-co-HFP	765	762	765	766	766
1200	$-CF_2$ group of PVDF-co-HFP	1207	1209	1211	1213	1216
1390	CF_2 - deformation of PVDF-co-HFP	1390	1388	1386	1389	1392

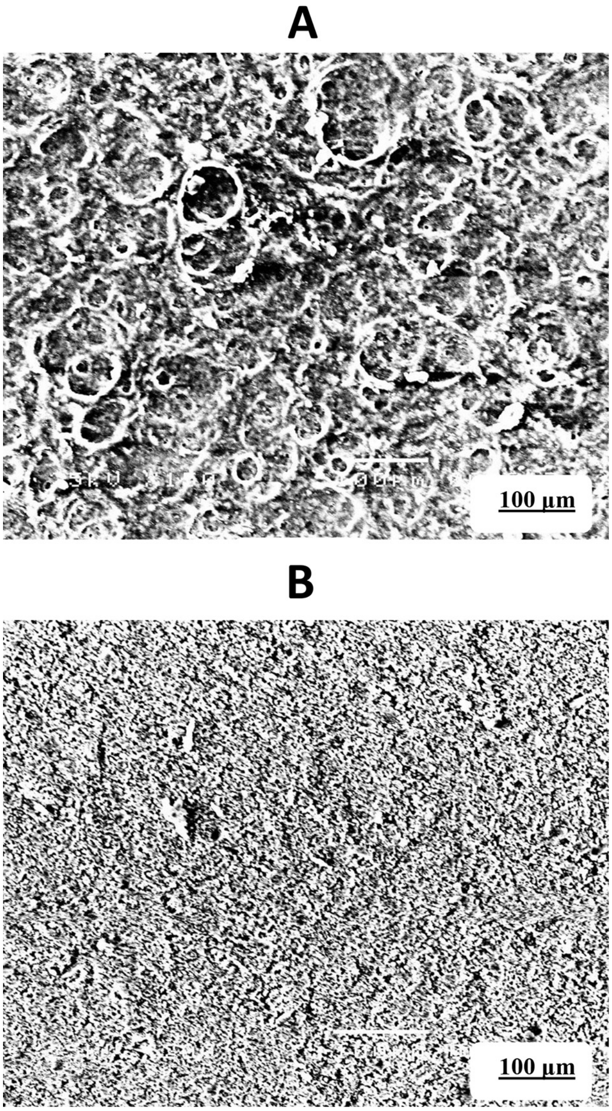

Fig. 6. SEM photographs of A) BOPCE and B) BOPCE containing 2 wt % $LiAlO_2$ (OPNCE).

co-HFP matrix in presence of PVAc, EC-DEC and $LiCF_3SO_3$ salt, Fig 6 A. This porous appearance disappears in presence of nano $LiAlO_2$ filler particles, Fig 6 B, showing the good homogeneous distribution within the matrix of the PVDF-co-HFP that may be the reason of the enhanced thermal stability nature of all $LiAlO_2$ samples.

3.5. *Electrical properties*

The temperature dependence of electrical conductivity (AC) of BOPCE and BOPCE containing different nano $LiAlO_2$ concentrations (2, 4, 6, 8 wt %) is investigated in a temperature range of 298–388 K and illustrated in Fig. 7. The figure shows that the AC-ionic conductivity of composites increases in general with temperature increase. Also, curves appear linear, so the apparent activation energy for the ions transport (E_a) are obtained using the Arrhenius model $\sigma = \sigma_0 \exp(-E_a/RT)$, where R, T, σ and σ_0 are gas constant, temperature, the AC-ionic conductivity and the pre-exponential factor, respectively. According to this equation, the activation energy for the ions transport can be calculated from the slope of imitated straight line, Table 2. From this table, it can be seen that the activation energy value changes with filler content to have a minimum value of 0.07 eV for the BOPCE containing 2 wt % of $LiAlO_2$, and a maximum one of 0.12 eV for the BOPCE containing 8 wt % of $LiAlO_2$. This can also show that the variation in $LiAlO_2$ filler content can influence the ionic conduction, Table 2. The values variation of AC-ionic conductivity at room temperature with the filler content can also be seen, Fig. 7. The figure showed that the AC-ionic conductivity at room temperature has the following order: σ_{Ac} (BOPCE, 2 wt % $LiAlO_2$) > σ_{Ac} (BOPCE, 6 wt % $LiAlO_2$) > σ_{Ac} (BOPCE, 4 wt % $LiAlO_2$) > σ_{Ac} (BOPCE, 8 wt % $LiAlO_2$) > σ_{Ac}(BOPCE). This variation behavior may be related to the suitable distribution of the filler particles within a definite matrix structure, to create suitable conduction pathways for Li^+- ions. The frequency dependence of dielectric constant (ε') and loss (ε'') at room temperature for BOPCE and BOPCE containing different nano $LiAlO_2$ concentrations is shown in Fig. 8 A,B. In general, it can be seen that ε' and ε'' decreases as frequency increases. This decrease is relatively fast at lower frequencies and slow at higher ones. The decrease in dielectric permittivity with frequency increasing can be associated to the inhability of dipoles to rotate rapidly leading to a lag between frequency of oscillating dipole and that of applied field [26]. Such high dielectric constant values can be attributed to the high ionic conductivity on account of the presence of $LiAlO_2$ nano particles and its good distribution within the co - polymer matrix and also due to the good interactions between the Lewis acidic sites on the surface of those particles and the ions of lithium tri fluoro methane sulphonate [27]. At the same time the dielectric loss decrease with frequency is due to the high periodic reversal of the field at the interface, the contribution of charge carriers (ions) towards the dielectric loss decreases with frequency increasing and this decreasing can be attributed to the reduction of the ions diffusion in the polymer matrix with frequency increase. More notably, the values of dielectric constant (ε') and loss (ε'') of all composites comes in the same order of AC- conductivity, where the BOPCE containing 2 wt % of $LiAlO_2$ showed the highest values (1×10^5 and

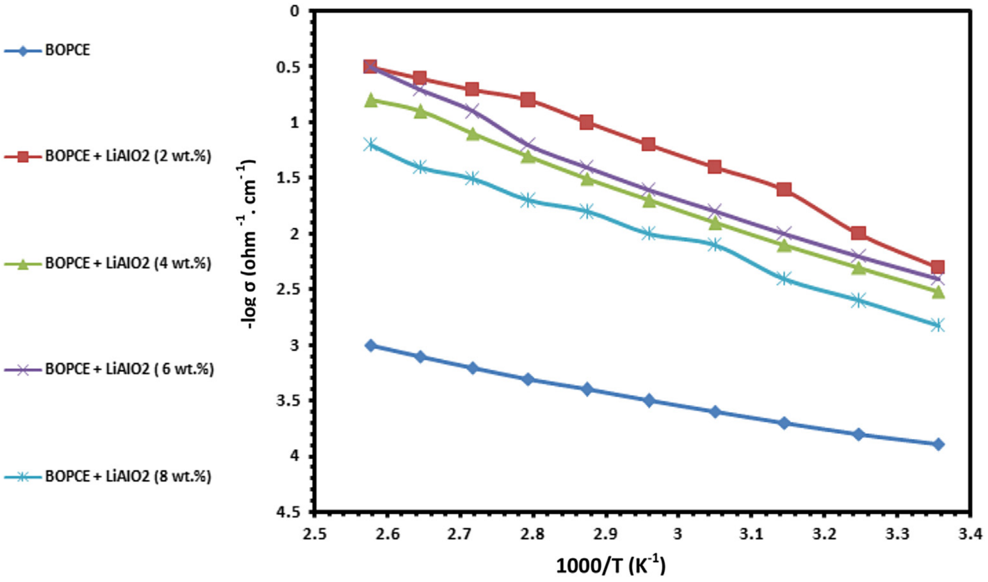

Fig. 7. Temperature dependent AC-ionic conductivity (100 Hz) plots of BOPCE and BOPCE containing different concentrations of $LiAlO_2$ (2, 4, 6, 8 wt %).

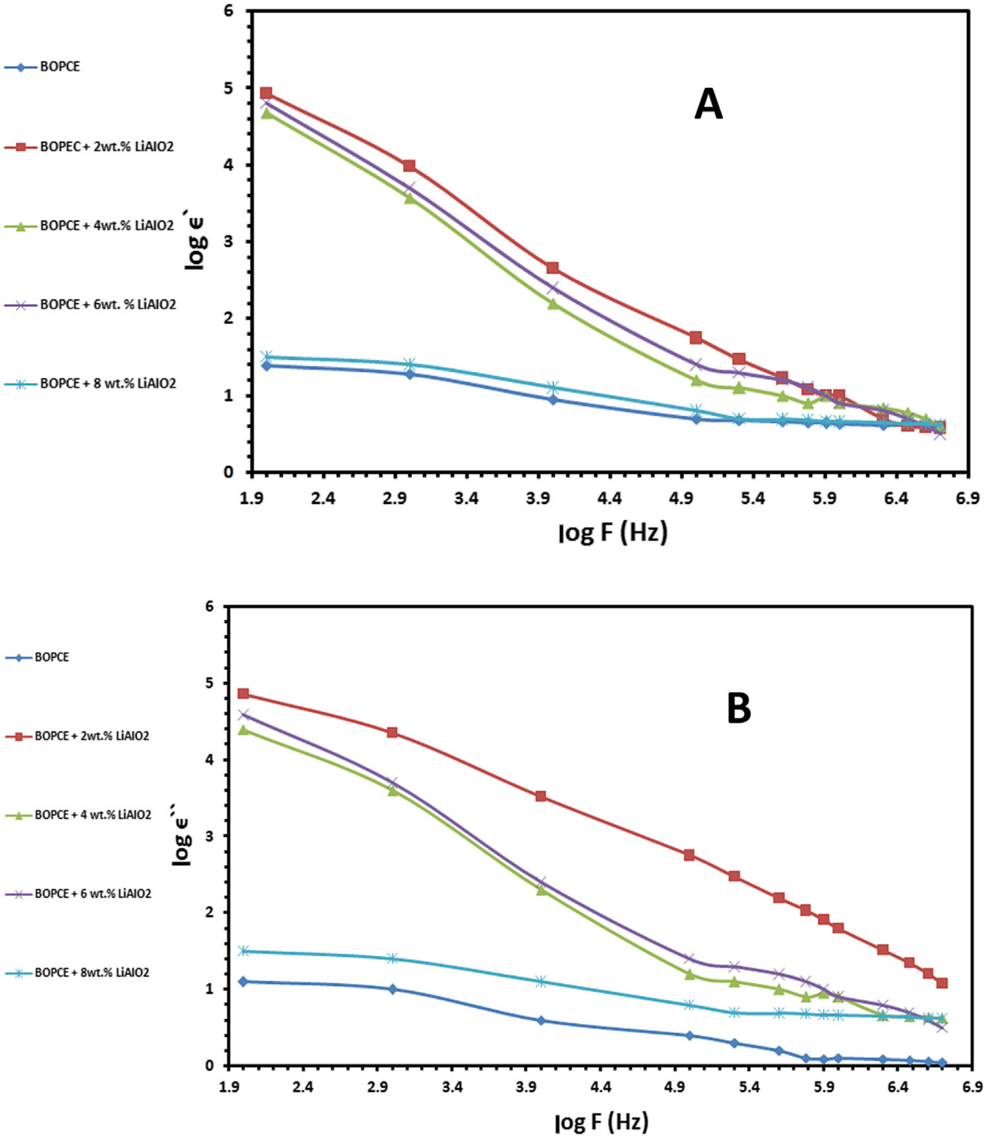

Fig. 8. Frequency dependent dielectric constant (A) and loss (B) plots of BOPCE and BOPCE containing different concentrations of $LiAlO_2$ (2, 4, 6, 8 wt %) at room temperature (298 K).

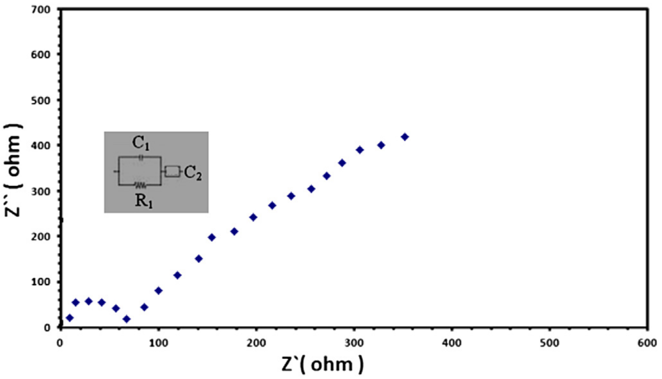

Fig. 9. Complex impedance of BOPCE containing 2 wt % $LiAlO_2$ (OPNCE) at room temperature (298 K).

79432.8 for dielectric constant (ε′) and loss (ε″) at 100 Hz, respectively).

Fig. 9 shows a complex impedance plot of OPNCE (BOPCE containing 2 wt % of $LiAlO_2$), the optimized sample of high electrical properties. The figure showed an impedance spectrum consists of a semi − circle and an inclined straight line. The semicircle is related to the conduction process and the linear region is due to the effect of the blocking electrode [28] that results in a charge polarization in the bulk of the copolymer, and represents the capacitance at the electrode and electrolyte interface [29]. Also, the value of bulk ionic conductivity was calculated to equal $5.15 \times 10^{-3}\ \Omega^{-1}\ cm^{-1}$ at room temperature. The equivalent circuit is also determined from the complex impedance spectrum and shown in Fig. 9. Where R1 is the bulk resistance of the electrolyte, C_1 is the bulk capacity of the electrolyte and C_2 is a capacity of bulk electrode − electrolyte interface.

To further show the high thermal stability nature (decomposition temperature value, T_d) of our optimized sample, a comparison with previous similar compositions [25,30,31] containing the same co − polymer matrix was established in Table 4.

3.6. Battery test

The electrochemical performance of OPNCE as a polymer electrolyte membrane for lithium ion batteries was evaluated in Li/$LiFePO_4$ half-cell, Fig. 10. The figure showed that the optimized sample can deliver a discharge capacity of around 140 $mAhg^{-1}$ for the first cycle and 125 mAh g^{-1} for the last one (50 th cycle) at 0.2 C, demonstrating a good cycle life.

The electrochemical behavior of the optimized sample makes it as a **promising** gel polymer electrolyte for lithium ion batteries application.

4. Conclusions

Gel polymer composites electrolytes and gel polymer nano composites electrolytes were prepared using solution cast technique. Each one was characterized using X-ray diffraction (XRD), thermal analysis (TG, DSC), Fourier transform infra −red spectroscopy (FT-IR) and scanning electron microscope (SEM). All characterization tools confirmed the effect of PVAc, $LiCF_3SO_3$ and $LiAlO_2$ on the crystalline structure and thermal stability behavior of all investigated composites electrolytes. The optimized sample containing 8 wt % of $LiCF_3SO_3$ salt showed the less crystalline structure ($X_c = 3.02\%$) compared to the other composites ones. The sample containing 2 wt % of $LiAlO_2$ showed the less crystalline structure ($X_c = 8.32\%$) and the highest conductivity value at room temperature ($4.98 \times 10^{-3}\ \Omega^{-1}\ cm^{-1}$). The AC-ionic conductivity, at room temperature and 100 Hz, has the following order: σ_{Ac} (BOPCE, 2 wt % $LiAlO_2$) > σ_{Ac} (BOPCE, 6 wt % $LiAlO_2$) > σ_{Ac} (BOPCE, 4 wt % $LiAlO_2$) > σ_{Ac} (BOPCE, 8 wt % $LiAlO_2$) > σ_{Ac} (BOPCE). The same sample showed high values of dielectric constant and loss at room temperature (1×10^5 and 79432.8 for dielectric constant and loss at 100 Hz, respectively), demonstrating the high ion orientation within the gel polymer composite electrolyte. The value of bulk ionic conductivity was also calculated to equal $5.15 \times 10^{-3}\ \Omega^{-1}\ cm^{-1}$ at room temperature. More importantly, the OPNCE sample showed a high decomposition temperature ($T_d = 362$ °C), revealing the high thermal stability of that sample. Also, the OPNCE sample was evaluated as a gel polymer electrolyte in Li/$LiFePO_4$ half cell at 0.2 C rate. It delivered a discharge capacity of around 140 mAh g^{-1} for the first cycle and 125 mAh g^{-1} for the last one (50^{th} cycle), demonstrating a good cycle life. This good conductive and thermally stable polymer nano composite electrolyte is a promised electrolyte for lithium ion batteries application.

Table 4
Comparison of decomposition temperature values of similar previous reported samples with our optimized sample (OPNCE).

Sample	T_d,°C	References
PVDF-co-HFP/EC-DEC/PVA/$LiCF_3SO_3$/$LiAlO_2$	362	This work
PVDF-co-HFP/EC-DEC/PVA/$LiBF_4$/$BaTiO_3$	310	[22]
PVDF-co-HFP/EC-PC/$Mg(ClO_4)_2$/MgO	250	[26]
PVDF-co-HFP/EC-PC/$LiCF_3SO_3$	80	[27]

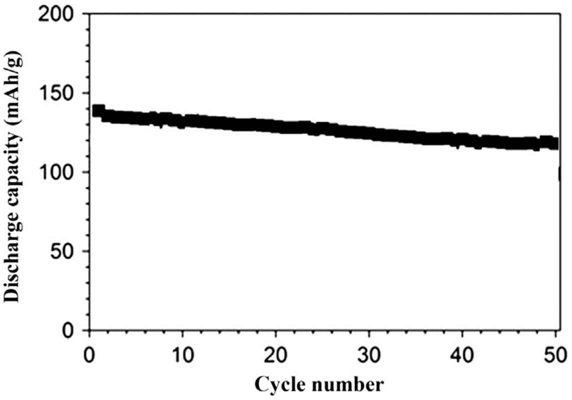

Fig.10. Discharge capacity against cycle number of BOPCE containing 2 wt. % $LiAlO_2$ (OPNCE) at room temperature (298 K), current rate = 0.2C.

Acknowledgment

I would like to introduce my grateful thanks to Benha University (http://www.bu.edu.eg/en/) for the financial support of this scientific research work through a competitive research project (Third stage, Project N. 10.) (4/1/C) titled as “Preparation and characterization of some polymer nano composites electrolytes for improved energy storage in lithium ion batteries”. Also, my sincere thanks to the lab group of IAM - KIT, Germany for helping in battery assembly using the glove box.

References

[1] J.Y. Sanchez, F. Alloin, C.P. Lepmi, Mol. Cryst. Liq. Cryst. 324 (1998) 257.
[2] G. Cheruvally, J.-K. Kim, J.-W. Choi, J.-H. Ahn, Y.-J. Shin, J. Manuel, P. Raghavan, K.-W. Kim, H.-J. Ahn, D.S. Choi, C.E. Song, J. Power Sources 172 (2007) 863–869.
[3] A.M. Stephan, Y. Saito, Solid State Ion. 148 (2002) 475–481.

[4] K.M. Kim, J.M. Ko, N.-G. Park, K.S. Ryu, S.H. Chang, Solid State Ion. 161 (2003) 121–131.
[5] V. Aravindan, P. Vickraman, Eur. Polym. J. 43 (2007) 5121–5127.
[6] D. Saikia, Y.W. Chen-Yang, Y.T. Chen, Y.K. Li, S.I. Lin, Desalination 234 (2008) 24–32.
[7] A. Manuel Stephen, K.S. Nahm, M.A. Kulandainathan, G. Ravi, J. Wilson, Eur. J. 42 (2006) 1728–1734.
[8] M.A. Ratner, D.F. Shriver, Chem. Rev. 88 (1) (1988) 109–124.
[9] N.-S. Choi, Y.-G. Lee, J.-K. Park, J.-M. Ko, Electrochim. Acta 46 (10–11) (2001) 1581–1586.
[10] O. Inganas, Polym. Int. 20 (3) (1988) 233–236.
[11] D.-W. Kim, J.-K. Park, H.-W. Rhee, Solid State Ion. 83 (1–2) (1996) 49–56.
[12] E. Morales, J.L. Acosta, Solid State Ion. 96 (1–2) (1997) 99–106.
[13] F. Croce, R. Curini, A. Martinelli, L. Persi, F. Ronci, B. Scrosati, R. Caminiti, J. Phys. Chem. B 103 (48) (1999) 10632–10638.
[14] D.E. Strauss, D. Golodnitsky, E. Peled, Electrochem. Solid State Lett. 2 (1999) 115.
[15] Emad M. Masoud, A.-A. Elbellihi, W.A. Bayoumy, M.A. Mousa, Alloy. Compd. 575 (2013) 223–228.
[16] Abdelhameed Ahmed ElBellihi, Wafaa Abdallah Bayoumy, Emad Mohamed Masoud, Mahmoud Ahmed Mousa, Bull. Korean. Soc. 33 (9) (2012) 2949–2954.
[17] Emad M. Masoud, Alloy. Compd. 651 (2015) 157–163.
[18] E.M. Masoud, A.-A. El-Bellihi, W.A. Bayoumy, M.A. Mousa, Mater. Res. Bull. 48 (2013) 1148–1154.
[19] R.B. Khomane, A. Agrawal, B.D. Kulkarni, Mater. Lett. 61 (2007) 4540.
[20] D. Saikia, A. Kumar, Electrochim. Acta 49 (2004) 2581–2589.
[21] Z. Li, G. Su, X. Wang, D. Gaw, Solid State Ion. 176 (2005) 1903.
[22] N.T. Kalyana Sundaram, A. Subramania, Electrochim. Acta 52 (2007) 4987–4993.
[23] L. Hu, Z. Tang, Z. Zhang, J. Power Sources 166 (2007) 226.
[24] H.P. Klug, L.E. Alexander, X – Ray Diffraction Procedures, Wiley, New york, 1970.
[25] M. Ulaganathan, R. Nithya, S. Rajendran, S. Raghu, Solid State Ion. 218 (2012) 7–12.
[26] A. Awadhia, S.K. Patel, S.L. Agrawal, Prog. Cryst. Growth Charact. Mater. 52 (2006) 61.
[27] H.M. Xiong, X. Zhao, J.S. Chen, J. Phys. Chem. B105 (2001) 10169.
[28] D. Shanmukaraj, G.X. Wang, R. Murugan, H.K. Liu, Phys. Chem. Solids 69 (2008) 243–248.
[29] Emad M. Masoud, M. Khairy, M.A. Mousa, Alloy. Compd. 569 (2013) 150–155.
[30] G.P. pandey, R.C. Agrawal, S.A. Hashmi, J. power sources 190 (2009) 563–572.
[31] A.M. Stephan, S.G. Kumar, N.G. Renganathan, M.A. Kulandainathan, Eur. Polym. J. 41(1), 15–21.